Degradation and recovery of solid oxide fuel cell performance by control of cathode surface acidity: Case study – impact of Cr followed by Ca infiltration

Han Gil Seo[1], Anna Staerz[1], Georgios Dimitrakopoulos[1,2], Dongha Kim[1], Bilge Yildiz[1,3], Harry L. Tuller[1]*

[1] *Department of Materials Science and Engineering, Massachusetts Institute of Technology, Cambridge, MA, 02139, USA*

[2] *Exponent, Inc., Natick, MA, 02139, USA*

[3] *Department of Nuclear Science and Engineering, Massachusetts Institute of Technology, Cambridge, MA, 02139, USA*

[*]*Corresponding author.*
E-mail address: tuller@mit.edu (H. L. Tuller)

Abstract

Solid oxide fuel cells (SOFC) have attracted attention as clean and efficient energy conversion devices with low emissions. However, several degradation mechanisms limit the electrochemical performance of current SOFCs, with cathode degradation due to Cr-poisoning from metal interconnects particularly problematic. The acidity/basicity of binary additives has been found to be a sensitive descriptor of the oxygen exchange kinetics, indicating that acidic Cr-species/basic Ca-species can be expected to deactivate/activate the cathode surface, respectively. Inspired by recent advances, the feasibility of relative acidity as a tool for reviving degraded SOFCs is demonstrated by neutralizing Cr-poisoned SOFCs by subsequent serial infiltration of Ca-species. A model mixed ionic and electronic conducting oxide, $Pr_{0.1}Ce_{0.9}O_{2-\delta}$ (PCO), is selected as the cathode material. Area-specific resistances (ASR) of symmetric cells obtained by electrochemical impedance spectroscopy show that Cr-infiltration results in a seven-fold increase in ASR, while subsequent infiltration of Ca-species leads to complete recovery. Performance degradation and recovery are attributed to depressed/enhanced redox properties at the PCO surface, as supported by XPS analysis. Experiments using anode-supported fuel cells show a reduction in peak power density by 26% upon Cr-infiltration, reversed following Ca-infiltration, after which no degradation is observed during subsequent operation for 100 h.

Keywords: solid oxide fuel cell; cathode Cr poisoning and recovery; oxygen reduction reaction; relative acidity; $(Pr,Ce)O_{2-\delta}$

1. Introduction

A major remaining challenge to making solid oxide fuel cells (SOFCs) suitable clean and efficient energy conversion devices with reduced emissions is addressing the well-known long-term chemical degradation in performance induced by chromia species generated from the fuel cell's steel alloy-based interconnects.[1–5] This Cr-induced degradation is largely reflected in a continuous decrease in the oxygen reduction reaction (ORR) kinetics at the fuel cell cathode. Although degradation rates of 0.2 - 0.5% per 1,000 hrs in single cells are acceptable today, significantly improved reliability and durability are required in practical fuel cell stacks operating under realistic conditions where 2-4-fold faster Cr-induced degradation rates are expected.[6,7] With a global SOFC market predicted to reach \$5.3 billion by 2028 [8], coupled with expensive projected SOFC replacement costs, developing means for reviving degraded performance would offer great value in rendering this technology commercially viable.

While Cr-induced degradation has received much attention, the exact mechanism in which absorbed Cr-species lead to the deactivation of actives sites for the ORR remains controversial.[2,5,9–11] Cr inevitably finds its way from the interconnect to the cathode surface via vapor phase or surface diffusion. Vaporized gaseous Cr-related phases, for example CrO_3 (g), CrO_2 (g), CrO (g), and Cr_2O_3 (s), can either deposit as large clusters or react with the segregated cations in the host cathode materials to form secondary compound phases, *e.g.* strontium chromates [5,9,11,12] In either case, such species are proposed to block active sites, thereby impeding the ORR. In our recent previous studies, however, we proposed an alternative explanation for the poisoning effect of CrO_x species on the ORR, which extends to other species such as SiO_x. We attributed this to the relative acidity of the additives associated with the induced depletion/accumulation of electrons e' at the electrode surface associated with whether the additive was acidic or basic relative to the electrode material [13]. Indeed, oxides that possess Smith acidities more acidic than the host mixed ionic and electronic conducting (MIEC) electrode were described as limiting electron charge transfer to adsorbed oxygen O_{ads}, and in turn oxygen incorporation into existing lattice vacancy sites $V_O^{\cdot\cdot}$ to form charge neutral O_O^x, as described by the following reaction.[13,14]

$$2e^{'} + V_O^{\cdot\cdot} + O_{ads} \rightarrow O_O^x$$

On the other hand, binary oxides infiltrated onto the host electrode that are more basic than the host cathode oxide, *e.g.* Li_2O and CaO, were demonstrated to exhibit faster ORR kinetics compared to the pristine electrode [10].

Herein, we selected $Pr_{0.1}Ce_{0.9}O_{2-\delta}$ (PCO) as an alternative model MIEC SOFC cathode material given that it is free of species such as Sr, common in perovskite-based cathodes (e.g. (La,Sr)(Co,Fe)O_3 (LSCF) [15,16] and Sr(Ti,Fe)O_3 (STF)) [17,18] that are known to segregate to the surface and lead to degradation of the surface ORR kinetics. This minimizes the difficulties in the interpretation of Cr-induced degradation by excluding intrinsic-driven poisoning (e.g. Sr segregation). In this regard, using PCO allowed us to systematically examine the effects of extrinsic Cr- or Ca-based surface additives on the area-specific resistance (ASR) of symmetric cells by electrochemical impedance measurements (EIS), as described in our preceding work.[19] While the Cr and Ca infiltration steps did not have a significant effect on the ohmic resistance of the cells, the polarization resistance associated with surface oxygen exchange processes was strongly influenced. We show that the magnitude of the total ASR markedly increased upon Cr-infiltration by a factor of 10, but then, it decreased by a subsequent Ca-infiltration by a factor of 2 compared to the pristine sample, although activation energies were little impacted as reported previously.[14,19]

Our findings reveal that the relative acidity/basicity at the oxide surface can be used as a guideline to recover degraded cathode and overall SOFC performance. To expand our previous studies in which the single acidic (Cr) and basic (Ca) additives were found to degrade or improve the polarization resistances, respectively, in this work, we further examine how serial infiltration of the basic Ca-additive can mitigate performance degraded by initial infiltration with the acidic Cr-additive. We first examine the ASR degradation and recovery of screen-printed PCO symmetric cells with the aid of EIS measurements. We then fabricate a Ni-YSZ anode-supported single cell with an yttria-stabilized zirconia (YSZ) electrolyte and a PCO cathode and evaluate the cell performance and stability while controlling the relative acidity of the PCO cathode infiltrates. For the latter cells, we demonstrate that an initial Cr-infiltration leads to a significant reduction in peak power density by 26% when the cells are operated at 650℃, but the subsequent infiltration of Ca-species was able to effectively reverse the Cr-degraded cell performance. Furthermore, the resulting recovered cell performance remained stable for a subsequent 100 h test. These findings demonstrate the reversibility of power output via controlled relative acidity that promises practical means for recovering and mitigating SOFC degradation.

2. Methods

2. 1 Fabrication of PCO symmetric cells and anode-supported single cells with PCO cathode.

A solution combustion route was used to synthesize the PCO powder, starting from nitrate-based $Ce(NO_3)_3\cdot 6H_2O$ (99.99%, Alfa Aesar), $Pr(NO_3)_3\cdot 6H_2O$ (99.99%, Alfa Aesar) precursors and citric acid. The calcined PCO powder was mixed with 70 μL of 1, 5-pentanediol (Alfa Aesar, 97%) as a solvent and 10 μL of Optapix PAF 35/water (50:50, Zschimmer & Schwarz Inc.) as a binder to form a slurry. For the preparation of PCO symmetric cells (PCO/YSZ/PCO), the resulting PCO slurry was screen-printed onto both sides of a YSZ (8 mol% yttria) (100) single crystal substrate (MTI, double side polished, 10 x 10 x 0.5 mm^3). It was then dried at 90 °C for 1 h and sintered at 1350 °C for 3 h under ambient air at a heating/cooling rate of 5 °C/min. Silver paste (Fuel Cell Materials) was used as current collector. The cell with the pristine PCO electrode was first measured to provide the reference ASR. The sample was then infiltrated with 0.15 at% Cr-species (as an acidic poison source) by using a Cr-nitrate ethanol-based solution with 0.002 M, as described in preceding works [14,19]. The resulting cell was then dried and re-loaded into the electrochemical setup. The cell was heated up to 650 °C and stabilized until it reached equilibrium. It was then followed by re-measurements of the electrochemical performance. The resulting/tested cell was subsequently serially infiltrated with 0.5 at% Ca-species (as a basic recovery source) by using a Ca-nitrate ethanol-based solution with 0.002 M and re-measured for comparison of the relative ORR activities.

A screen-printed PCO cathode (~15-μm thick) was deposited on a commercial Ni-YSZ (400-μm thick) anode-supported single cell with a YSZ (8 mol% yttria) (3-μm thick) electrolyte and Gd-doped ceria ($Gd_{0.1}Ce_{0.9}O_{1.95}$, GDC) buffer layer (3-μm thick) (Fuel Cell Materials, AEB-2.0), which in turn configures a Ni-YSZ/YSZ/GDC/PCO. The detailed deposition for the PCO cathode is described above. Three different single cells were prepared; the pristine, Cr-infiltrated, and Cr-/Ca-infiltrated samples. All infiltrations were performed prior to pasting current collectors. After each infiltration, the heat treatment at 650 °C for 2 h was conducted. Silver paste was then applied to both electrodes as current collector prior to loading the cell into the reactor. The pristine, Cr-infiltrated, and Cr-/Ca-infiltrated PCO-based single cells were evaluated respectively for comparison of peak power densities. Because this study was designed to investigate the relative impact of acidic and basic additives on fuel cell performance, no effort was made to obtain exceptional fuel cell performance with the reference cell.

2. 2 Physical and chemical characterization

The microstructures of anode-supported single cells with PCO cathode were examined both prior and subsequent to infiltrations by a Zeiss Merlin High-Resolution scanning electron microscope (SEM). The local chemical information at the PCO surface of the Cr-infiltrated and Cr-/Ca-infiltrated single cells was analyzed by X-ray photoelectron spectroscopy (XPS) using a Physical Electronics Versaprobe II spectrometer equipped with a monochromated Al K-alpha X-ray source with 1486.68 eV by examining and analyzing the XPS spectra associated with O 1s, Cr 2p, and Ca 2p levels.

2. 3 Electrochemical characterization

The electrochemical performance of the pristine, Cr-infiltrated, and Cr-/Ca-infiltrated symmetric cells was investigated by EIS with the aid of a Solatron 1255 HF frequency response analyzer, interfaced with an EG&G PAR potentiostat model 273A. The cells were placed inside of an alumina tube under gas mixtures of O_2 and N_2 controlled by digital mass flow controllers. Impedance spectra with an AC perturbation of 20 mV in the frequency range of 0.01 Hz to 1 MHz were obtained in the temperature range of 500-650℃at oxygen partial pressures (pO_2) between 0.1 and 1 atm. A distribution relaxation of time (DRT) analysis of impedance spectroscopy was undertaken with DRT tools and software [20,21] to investigate the characteristic processes in more detail.

The cell performances of the pristine, Cr-infiltrated, and Cr-/Ca-infiltrated PCO-based single cells were evaluated using a button-cell reactor.[22] A ceramic adhesive (Ceramobond 552-VFG, Aremco) was employed to seal the cells. The cells were heated up to 650 ℃ with a heating rate of 1 °C/min under Ar and air at the anode and cathode, respectively, and then followed by the reduction of the anode under pure dry hydrogen for 1 h. Then, humidified hydrogen (3% H_2O – 97% H_2) as the fuel and air as the oxidant were applied to the anode and cathode, respectively, for additional 2 h prior to the measurements. Impedance spectra were recorded using a PARSTAT 4000A Potentiostat (AMETEK Inc.) under open circuit voltage (OCV) in the frequency range of 0.05 Hz - 1 MHz with an AC perturbation of 15 mV. The typical I-V and I-P curves of the cells were collected at operating temperatures from 550 to 650 ℃ with intervals of 50 °C. The stability of current and peak power densities of the Cr-/Ca-infiltrated PCO-based single cell was measured under a constant voltage of 0.75 V at 650 °C for 100 h. A relatively low current density corresponding to 0.75 V was chosen to avoid potential internal temperature increases, depletion of fuel supply, and partial re-oxidation of the Ni [23].

3. Results and Discussion

3.1 Degradation and recovery of polarization resistance of symmetric cells with controlled acidity

As in our previous study, where we examined the impact of individual acidic (Cr-species) and basic (Ca-species) additives on the ASR of PCO/YSZ/PCO symmetric cells, a pristine cell serves as the reference [19]. Note that we have clearly shown in previous studies that infiltration treatments can be used to accelerate poisoning effects in a manner similar to that achieved by exposure to atmospheres containing vaporized Cr-species [14,19]. To ensure clear and substantial initial degradation in performance by Cr-species, 0.15 at% Cr-species (over four times the concentrations found by Menzler *et al.* after 3,000 h of stack operation [24]) were first infiltrated into both sides of the PCO electrodes and the resulting cell performance re-measured. The tested Cr-poisoned cell was subsequently infiltrated with 0.5 at% basic Ca-species and re-measured. **Fig. 1a** shows typical Nyquist plots of the pristine, Cr-infiltrated and Cr-/Ca-infiltrated PCO symmetric cells obtained at 600 °C. Impedance spectra were fitted with three serial *R-Q* circuit elements. Note that the ohmic resistance in the range of 29.51 – 30.66 Ω·cm^2, that corresponds mainly to the YSZ electrolyte, is omitted from the present spectra to clarify the impact of the additives on the rest of the impedance spectra. The remaining total ASR (ASR_{total}) can be characterized by two semicircles that we designate as high frequency (HF) and low frequency (LF) contributions – see peak frequency designations in Fig. 1a. The characteristic resistances (sum of R_{HF} and R_{LF}), approximated by the sum of the diameters of the two semicircles, were found to increase nearly seven-fold as a result of the Cr-infiltration. Upon subsequent infiltration of the Cr-poisoned cell by Ca, ASR_{total} showed a five-fold decrease, nearly returning to the initial value of that of the pristine cell. The Nyquist plots of the impedance spectra, however, are observed to be somewhat distorted from ideal semicircles as a result of several overlapping processes in the frequency regime of interest. In order to better differentiate the various processes characterized by different relaxation times, the DRT approach was applied that enables the characteristic peaks to be more readily distinguished as observed in **Fig. 1b**. The resulting DRT spectra shows that while the peaks in the HF regime are little dependent on infiltration, the LF peaks exhibit a strong dependency on infiltration, consistent with those observed in the Nyquist plots. Given that the HF contributions are likely associated with ion transfer processes across the electrolyte-cathode interface [25,26], it is not surprising that the resistances in the HF regime are not sensitive to infiltration. On the other hand, the serial infiltration of Cr and Ca had a significant impact on the LF characteristics, that are more likely associated with the surface oxygen exchange processes.[27,28] The tallest peak of the Cr-infiltrated PCO cell appears in the LF regime, characteristic of Cr-poisoned surfaces. Since Cr-infiltration is expected to impede the rate of oxygen reduction reaction at the surface, the additional peak related to the Cr-poisoned surface appears at the longest relaxation times (Fig. 1b). Arrhenius plots of the resulting ASR_{total} and ASR_{LF} of the pristine, Cr-infiltrated and Cr-/Ca-infiltrated PCO symmetric cells are shown in **Fig. 1c**. As expected, little change is observed in the activation energies (E_a) associated with these parameters with $E_a \sim 1.35$ - 1.43 eV as reported previously for acidity impacted ORR kinetics.[14,19] The polarization resistances in the LF regime predominantly contribute to the overall cathode performance. In this study, the reason for limiting the temperature window down to relatively lower temperatures below 650℃ is due to the thermally activated processes, making it more difficult to measure the resistance associated with the surface exchange process at higher temperatures such as the typical operating temperature of 800℃. However, similar mechanism of poisoning and recovery are expected and can be extrapolated to higher temperatures due to the fact that there is no significant change in activation energies regardless of infiltration of additives. Indeed, measurements at these lower temperatures remain relevant given reports of significant Cr-vaporization remaining active under these conditions.[29–33] Opila et al. reported that the rate of Cr-volatility was already high enough at 600 °C to measure significant levels of vapor phase Cr transport [29] while Asteman et al. showed that $CrO_2(OH)_2(g)$ evaporation from

Cr_2O_3-forming austenitic steel is substantial at temperatures as low as 600 °C [30]. Furthermore, Spotorno et al. reported significant weight gain of a Cr-related oxide layer even at a temperature of 650 °C (e.g. 30 μg·cm^{-2} for 250 h).[33] Taken together, the referenced studies confirm that Cr-poisoning remains active at these lower temperatures and so the findings of the present studies remain relevant both for cells operating at higher temperatures and for future cells that may operate efficiently at intermediate temperatures.

In preceding work, it was demonstrated that while CaO itself is inert to ORR, it serves to induce the accumulation of electrons at the PCO surface due to its lower work function relative to that of PCO, thereby enhancing the catalytic activity of the PCO cathode. For this reason, we attributed the observation of Cr-degradation and Ca-enhancement in ORR kinetics to an electronic coupling between the additives and PCO, that is, acidic Cr-additives lead to the depletion of surface electrons, while basic Ca-additives lead to electron-accumulation. This allowed us to suspect that one might be able to compensate for surfaces depleted in electrons by *e.g.* acidic Cr-infiltration, by subsequent infiltration with a more basic additive like CaO. As demonstrated in the results summarized in Fig 1a-c, this hypothesis was indeed confirmed. These results therefore have important implications for the capability to extend the lifetime of SOFCs and therefore their commercial viability by demonstrating the ability to recover initial fuel cell performance following degradation without having to replace key fuel cell components.

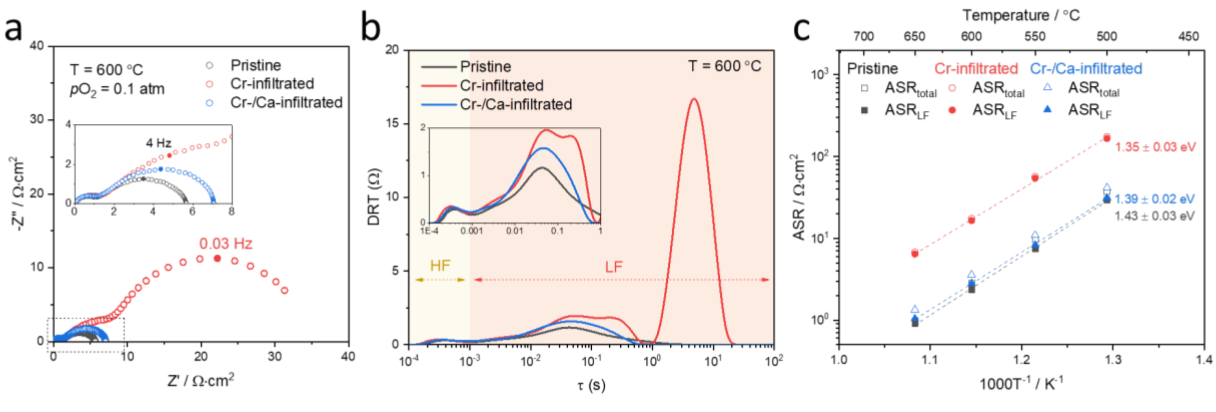

Fig. 1 (a) Typical impedance spectra and (b) distribution of relaxation time (DRT) plots of the PCO/YSZ/PCO symmetric cells (pristine and with serial infiltration of Cr-and Ca-additives) measured at 600°C. (c) Arrhenius plot of the total (ASR_{total}) and LF (ASR_{LF}) polarization resistances.

3.2 Local surface chemistry of Cr- and Cr-/Ca-infiltrated PCO-based single cells.

Fig. 2a presents the cross-sectional SEM image of an anode-supported cell with a Ni-YSZ anode, a YSZ electrolyte, a GDC buffer layer and a PCO cathode (denoted as Ni-YSZ/YSZ/GDC/PCO).

The sintering procedure resulted in a homogeneous highly porous PCO layer with a grain size of approximately 500 nm. Although chromia and calcia were successively infiltrated into the PCO layer, no significant change in morphology was observed, as shown in the magnified images in **Figs. 2b and c**. This is due to the low concentration of loading levels relative to that of the host PCO layer. Despite the low level of infiltrants, Cr and Ca elements were detected by XPS. The detailed XPS spectra associated with O 1s, Cr 2p, and Ca 2p levels of Cr- and Cr-/Ca-infiltrated PCO-based single cells are shown in **Figs. 2d-f**. For the O 1s spectra, two main peaks are observed, that have previously been assigned to oxygen bound to Ce(III) and Ce(IV) at high and low binding energies, respectively. [34,35] While the ratio of Ce(III)/Ce(IV), as reflected by the respective areas under the fitting curves, was found to be roughly 0.29 in the Cr-infiltrated single cell, it increased significantly to 1.08 with serial infiltration of Ca-species (**Fig. 2d**). Similarly, both Cr(VI) and Cr(III) peaks, assigned to high and low binding energies, respectively, were detected in the Cr-/Ca-infiltrated cell, showing that serial infiltration of Ca-species led to enhancement in the Cr(VI)/Cr(III) ratio, from 0.90 to 1.56, as presented in **Fig. 2e**. According to Smith acidity scale, acidic Cr-species can deplete the surface electrons of PCO, thereby inducing oxidation of Pr(III) to Pr(IV) that is in the same direction as the observed increase in the Ce(IV)/Ce(III) ratio. On the other hand, Ca-infiltration results in the accumulation of surface electrons, enabling instead reduction of Pr(IV) to Pr(III), followed as well, by occupation of the higher lying Ce 4f level.[36] This is further consistent with our earlier observations of changes in the magnitude of the electrical conductivity of PCO specimens following serial infiltration, i.e. decreases under acidic Cr and increases under basic Li infiltration respectively.[14] Furthermore, the reduction in activation energies of conductivity of PCO specimens upon Li-infiltration was previously observed and related to small polaron hopping induced in the Ce 4f band.[14,37] The increase in the concentration of Cr(VI) upon Ca-infiltration would be consistent with the formation of $CaCrO_4$, thereby tying up the acidic CrO_x species. Two major binding energies of Ca 2p peaks were detected in Cr-/Ca-infiltrated cell (**Fig. 2f**), further supporting the notion that successive infiltration of Ca-species leads to the recovery of Cr-poisoned performance. We additionally performed X-ray diffraction analysis to investigate whether or not Cr-species can be doped into the PCO lattice. PCO and mixed PCO-Cr_2O_3 powders were prepared and annealed at 1000°C for 12 h in air. For the latter, no secondary phases were observed and the calculated lattice parameters of PCO from the two prepared powders remained nearly identical (within a small error of < 0.01% (not shown here)). There was thus no evidence of any significant Cr dissolution into the PCO. This is consistent with both the poor cation size match of Ce vs Cr and also the generally extremely low cation diffusivity of impurities in zirconia and ceria. [38,39] For example, based on the bulk diffusion coefficient of Ca in zirconia, estimated at ~ 10^{-22} cm^2s^{-1} at 800℃ [38], the estimated bulk diffusion length for 100 h is only 0.06 nm. Given measurement temperatures below 650℃ in this work, Cr and Ca-species are not expected to enter the PCO lattice to any measurable degree. Taken together, our finding illustrates that the surface chemistry of mixed conducting electrodes can be manipulated to impact electronic coupling between the additives and PCO, ultimately leading to the recovery of Cr-

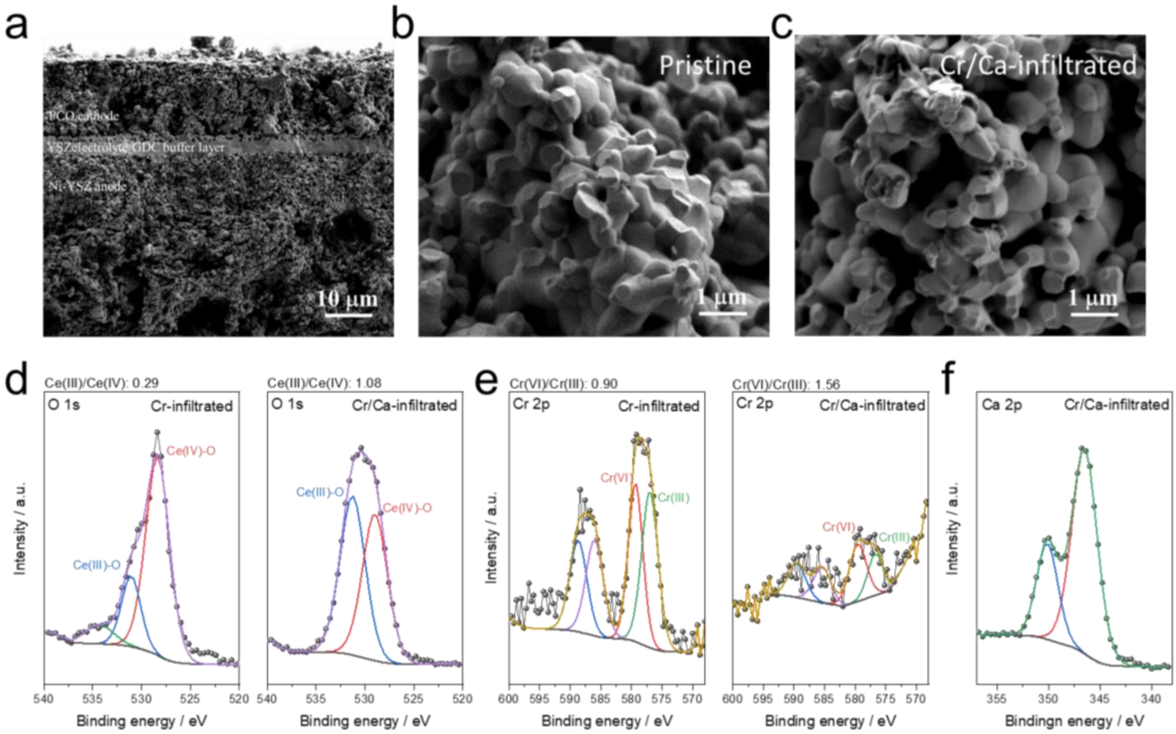

poisoned cell performance.

Fig. 2 (a) Cross-sectional SEM image of a Ni-YSZ/YSZ/GDC/PCO anode-supported single cell. Magnified SEM images of (b) the pristine and (c) the Cr-/Ca-infiltrated PCO cathode after fuel cell measurements. Comparison of XPS spectra of (d) O 1s and (e) Cr 2p for the Cr-infiltrated and Cr/Ca-infiltrated single cells. XPS spectra of (f) Ca 2p for the Cr/Ca-infiltrated single cell.

Based on both our observations (i.e. electronic coupling between the host oxide and additives) and other perspectives (i.e. blocking effect) previously reported,[40] mechanisms of Cr-poisoning at different Cr-concentrations and the proposed recovery strategy can be illustrated as shown in Fig. 3. The exchange reaction at the pristine surface is observed to depend on the rate of O_2 adsorption/dissociation and electron transfer from the electrode (middle image). At high levels of Cr-species, the surface adsorption of oxygen molecules on the cathode, followed by the electron charge transfer step, are hindered due to physical blocking by the electronically insulating Cr-rich layers (top left image). On the other hand, at low levels, the depletion of surface electrons induced by acidic Cr-additives significantly impedes the rate of oxygen exchange, while allowing for O_2-adsorption (top right image). Both cases degrade overall performance. For recovery of heavily Cr-poisoned surfaces, the addition of basic species can react with the Cr-species, forming a more porous calcium chromate layer (bottom left image) resulting in the recovery of the initially degraded performance as suggested by Zhao et al. for the recovery of Si-poisoning with La-additives.[34] For low concentrations of surface Cr-species, the serial addition of basic additives like CaO, not only enhances the ORR activity by inducing the accumulation of electrons in vicinity of surface Ca-species, but also compensates for the depleted electrons below the Cr-species, by neutralizing the initially acidic Cr-poisoned surfaces (bottom right image). The calcium chromate product formed is expected to exhibit intermediate levels of acidity that should serve to mitigate the electron depletion induced by the more dilute Cr-species.

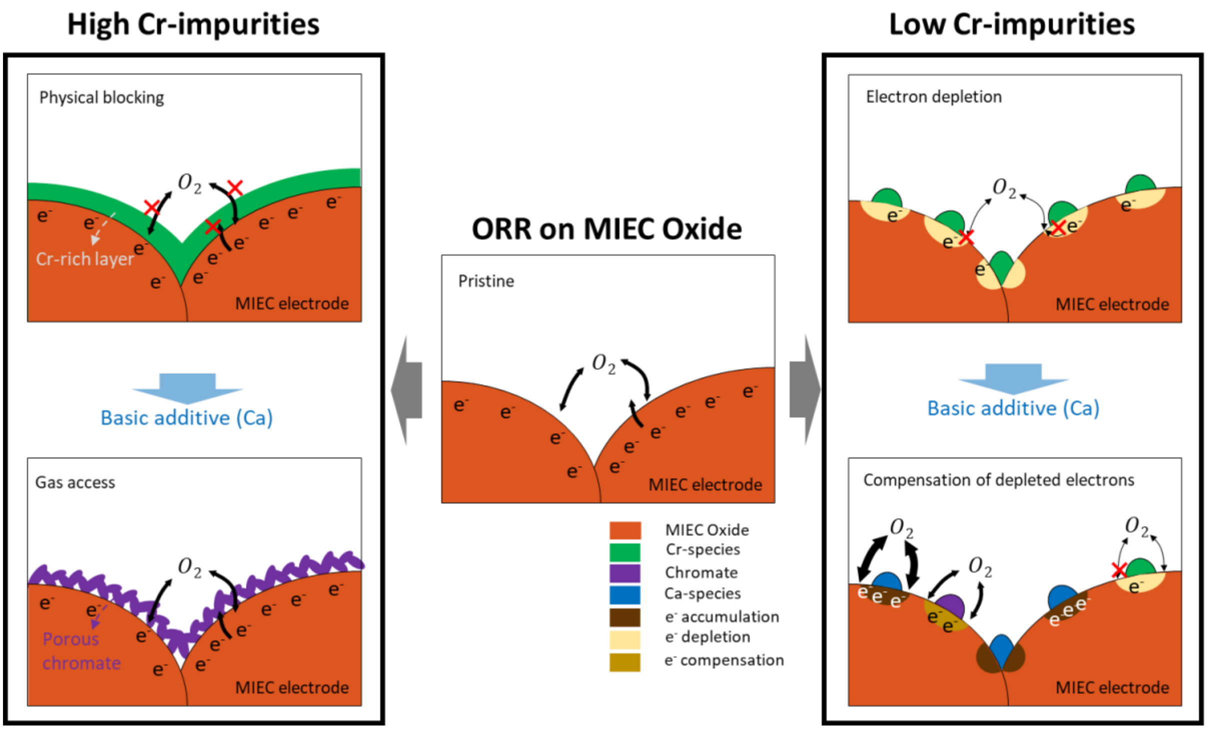

Fig. 3 Schematic illustration of Cr-poisoning mechanisms at different concentration levels and the strategy to achieve recovery by subsequent infiltration with CaO species. See text for further discussion.

3.3 Demonstration of anode-supported single cells with controlled acidity and stability

While measurements of the impact of acidic/basic infiltrants on oxygen exchange kinetics by conductivity relaxation and on the ASR of symmetric cells are clear indicators of their impact on the ORR kinetics of SOFC cathodes, it is instructive to demonstrate their impact directly on SOFC performance. Therefore, to directly demonstrate the feasibility of the use of controlled acidity as a tool for recovering degraded fuel cell devices, we evaluate in this study the fuel cell performance of anode-supported Ni-YSZ/YSZ/GDC/PCO single cells both prior to and following the infiltration of Cr- and Ca-species. Current (*I*)-voltage (*V*)-power density (*P*) *I-V-P* curves were recorded at 650°C under humidified H_2 (3% H_2O-97% H_2) as the fuel and dry air as the oxidant. The *I-V-P* measurements were first recorded with the pristine PCO cathode, then followed by Cr-infiltration and subsequent Ca-infiltration (**Fig. 4a**). The Cr-infiltrated single cell exhibits a peak power density of ~135 mW·cm^{-2} at 650ºC, considerably lower than that of the pristine cell under identical operating conditions (~182

$mW{\cdot}cm^{-2}$). This approximately 26% reduction in cell performance should be considered severe given that acceptable Cr-induced degradation rates of cells are reportedly 0.2-0.5% per 1,000 h. [6] Remarkably, this heavily Cr-degraded cell, when subsequently followed by an additional Ca-infiltration step, led essentially to the full recovery of the peak power density of the cell, reaching a value of ~184 $mW{\cdot}cm^{-2}$, nearly identical to that of the pristine cell, as summarized in **Fig. 4b**. To the best of our knowledge, this ability to reactivate degraded fuel cell performance using controlled acidity is demonstrated for the first time in SOFC cells.

Next, we attempt to isolate the source of the initial Cr-induced degradation and subsequent Ca-induced recovery of fuel cell performance by examining the frequency dependent impedance response of the overall cell. **Fig. 4c** shows that the overall cell performance is determined by both ohmic and polarization losses. We note that the ohmic losses, that we expect result from a superposition of the a) inherent Au lead wire resistances, b) the ohmic resistances of the composite YSZ/GDC electrolyte, and c) the series electronic resistance of the PCO cathode, given its rather low electronic conductivity [41], show little dependence on infiltration. However, the polarization losses of the PCO cathode are observed to be significantly influenced by infiltration, as reported above, similar to the symmetric cells. Focusing on the polarization resistance (R_{pol}) shown in **Fig. 4d** with respect to the observed degradation and recovery of performance (rather than the ohmic resistance (R_{ohm})), we first observe a ~2-fold increase in R_{pol} after Cr infiltration followed by a ~2-fold recovery achieved by the subsequent Ca infiltration, without significant changes in the respective activation energies. Although the infiltration step contributes to a change in R_{pol}, the change in power output at lower temperatures is not as pronounced as in R_{pol}, as shown in Fig. 2b. This is because the fraction of R_{total}, as reflected in R_{pol}, decreases as the temperature decreases. For example, a ~53% increase in R_{total} at 650℃ upon Cr-infiltration only contributes to a ~29% increase at 550 ℃. One can expect to observe considerably stronger contributions from R_{pol} once ohmic losses are minimized, for example, by use of shorter leads, by further optimization of electrode microstructure and/or utilization of composite cathodes to support enhanced electronic conducting pathways within the PCO cathode. For example, we recently were able to demonstrate high performance PCO-based single cells by optimizing cathode microstructure, exhibiting ~920 $mW{\cdot}cm^{-2}$ at 600 ℃. [41]

To test whether the recovered cell performance is maintained following Ca-infiltration, the stability of current and power densities of the recovered cell was further tested at 600℃ under a constant voltage of 0.75 V. **Fig. 4e** shows that no notable degradation was observed following 100 h of operation. These results again point to controlled acidity at the mixed conducting oxide surface as central to addressing chemically-driven degradation due to extrinsic poisoning sources. Obviously, tests of cells with much longer operating times will be required to further confirm these initial observations.

In this work, we successfully demonstrate the feasibility of fully recovering Cr-degraded

SOFC performance associated with chromia acidity through the subsequent addition of basic calcia additives. While our findings offer a conceptual advancement in demonstrating, for the first time, the ability to recover the performance of single fuel cell devices following chromia poisoning, further work is required to demonstrate how to successfully integrate the proposed concept into practical SOFC cells and stacks. For example, one could well imagine the application of periodic vapor phase treatments of SOFC stacks containing species that serve to deposit CaO onto the cathode surfaces to recover chromia induced degraded SOFC cathode performance. The feasibility of such an approach would appear to be supported by work performed by Han et al. who developed highly effective CaO@Al_2O_3 nanocomposite structures for CO_2 sorbents [42], while Natesan et al. reported the development of CaO coatings applied on V-4Cr-4Ti alloy for liquid metal blankets in fusion reactors, both via chemical vapor deposition methods [43].

The initial selection to demonstrate the principle of SOFC performance recovery following chromia poisoning with PCO as cathode rather than a more conventional perovskite electrode like LSCF may seem at first surprising. However, the lack of intrinsic degradation due to Sr segregation to the surface of PCO, in contrast to that of the common perovskite electrodes, allows for a much clearer understanding of the acid/base phenomena presented here. Nevertheless, while not demonstrated in this study, we have recently demonstrated in another study [41] that SOFC cells with PCO cathodes, when properly optimized, can also achieve exceptional peak power outputs, *e.g.* 0.92 Wcm^{-2} at the reduced temperature of $600°C$ by overcoming limitations in PCO's electronic conductivity with the aid of microstructural optimization. As pointed out in that study, high performance Co-containing perovskite oxides (*e.g.* LSCF) as cathode rely on the use of the element Co that is showing rapidly increasing demand as a key component of Li-battery cathodes, leading to inevitable increases in cost and depressed availability. Further considerations related to cost and integration of PCO into practical cells are described in our recent report [41].

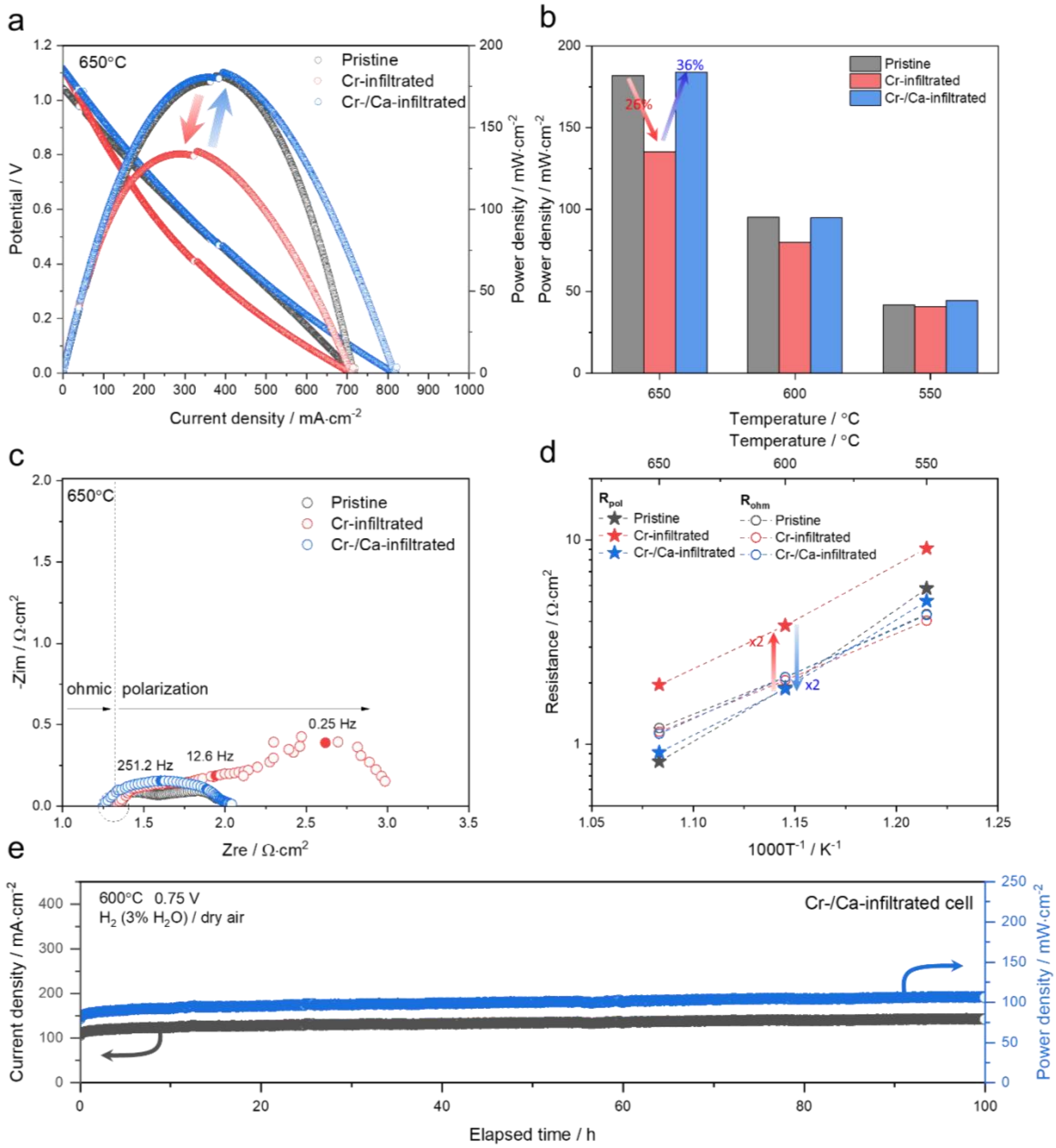

Fig. 4 (a) Typical I-V-P curves of the pristine, Cr-infiltrated and Cr-/Ca-infiltrated single cells at 650℃ under wet H_2 at the anode and the air at the cathode. Note that *I* denotes the current density, *V* is the potential, and *P* is the power density. (b) Comparison of the resulting peak power densities between the cells at T = 550 – 650 °C. (c) Impedance spectra of three different cells at 650 °C. (d) Temperature dependence of resistance values corresponding to the ohmic (R_{ohm}) and polarization (R_{pol}) resistance, respectively. (e) Long-term stability test of the single cell with Cr-/Ca-infiltrated PCO cathode for 100 h measured at 650℃ under a constant voltage of 0.75 V.

4. Conclusions

Both symmetric cells of the type air/PCO/YSZ/PCO/air and single SOFC cells of the type (H_2/H_2O)/Ni/YSZ/GDC/PCO/air were examined by impedance spectroscopy and the latter as well with respect to their current (*I*)-voltage (*V*)-power density (*P*) *I-V-P* curves as a function of treatment of the PCO electrode with acidic Cr-species followed by basic Ca-species. As expected, based on our earlier studies, the acidic Cr-infiltrant led to significant increases in cell impedance and a significant degradation by over 26% in cell power output. Of major significance for extended fuel cell life span, subsequent infiltration by Ca-species was able to recover the pristine cells' initial ASRs and peak power density. Our findings are expected to considerably extend SOFC useful lifetimes and thereby enhance the practical introduction of this promising energy conversion technology, characterized by high chemical to electrical energy efficiencies and considerably reduced emissions. While PCO was selected as a model system, without the objective of demonstrating record-high SOFC performance, we were able for the first time to demonstrate the feasibility of applying our acidity/basicity model as a tool for recovering SOFC peak power output following chromia poisoning. Further progress along these lines, both in terms of methods for integrating this concept in SOFC operation, and in extending it to a broad range of electrode materials, can be therefore be expected.

Acknowledgments

The research described in this work was initially supported by the US Department of Energy (DOE), National Energy Technology Laboratory (NETL), Office of Fossil Energy under Award no. DE-FE0031668— Robust highly durable solid oxide fuel cell cathodes – Improved materials compatibility & self-regulating surface chemistry. The work of H.G. Seo was supported, in part, by the National Research Foundation of Korea (NRF) grant funded by the Korea government (MSIT) (No.2021R1A6A3A03044464). We acknowledge the use of SEM and XPS in the MIT Materials Research Laboratory Shared Experimental Facility.

References

[1] M. Kornely, N.H. Menzler, A. Weber, E. Ivers-Tiffée, Degradation of a High Performance SOFC Cathode by Cr-Poisoning at OCV-Conditions, Fuel Cells. 13 (2013) 506–510. https://doi.org/10.1002/fuce.201200182.

[2] S.P. Jiang, X. Chen, Chromium deposition and poisoning of cathodes of solid oxide fuel cells - A review, Int. J. Hydrogen Energy. 39 (2014) 505–531. https://doi.org/10.1016/j.ijhydene.2013.10.042.

[3] K. Chen, N. Ai, K.M. O'Donnell, S.P. Jiang, Highly chromium contaminant tolerant BaO

infiltrated La 0.6 Sr 0.4 Co 0.2 Fe 0.8 O 3−δ cathodes for solid oxide fuel cells , Phys. Chem. Chem. Phys. 17 (2015) 4870–4874. https://doi.org/10.1039/c4cp04172k.

[4] Y. Niu, Y. Zhou, W. Lv, Y. Chen, Y. Zhang, W. Zhang, Z. Luo, N. Kane, Y. Ding, L. Soule, Y. Liu, W. He, M. Liu, Enhancing Oxygen Reduction Activity and Cr Tolerance of Solid Oxide Fuel Cell Cathodes by a Multiphase Catalyst Coating, Adv. Funct. Mater. 31 (2021) 1–11. https://doi.org/10.1002/adfm.202100034.

[5] H. Zhang, K. Xu, F. He, Y. Zhou, K. Sasaki, B. Zhao, Y. Choi, M. Liu, Y. Chen, Surface Regulating of a Double-Perovskite Electrode for Protonic Ceramic Fuel Cells to Enhance Oxygen Reduction Activity and Contaminants Poisoning Tolerance, Adv. Energy Mater. 12 (2022) 2200761. https://doi.org/https://doi.org/10.1002/aenm.202200761.

[6] S.D. Vora, U.S. DOE Office of Fossil Energy Solid Oxide Fuel Cell Program-19th Annual Solid Oxide Fuel Cell (SOFC) Project Review Meeting, 2018.

[7] M.M. Whiston, I.M.L. Azevedo, S. Litster, C. Samaras, K.S. Whitefoot, J.F. Whitacre, Meeting U.S. Solid Oxide Fuel Cell Targets, Joule. 3 (2019) 2060–2065. https://doi.org/https://doi.org/10.1016/j.joule.2019.07.018.

[8] Solid Oxide Fuel Cell Market to Hit USD 5.31 Billion in 2028; Increasing need to reduce Carbon Emissions and High Energy Demand to Boost Growth: Fortune Business Insights, Fortune Bus. Insights. (2021). https://www.fortunebusinessinsights.com/industry-reports/solid-oxide-fuel-cell-market-101306.

[9] S.P. Jiang, Y. Zhen, Mechanism of Cr deposition and its application in the development of Cr-tolerant cathodes of solid oxide fuel cells, Solid State Ionics. 179 (2008) 1459–1464. https://doi.org/10.1016/j.ssi.2008.01.006.

[10] Y. Chen, S. Yoo, X. Li, D. Ding, K. Pei, D. Chen, Y. Ding, B. Zhao, R. Murphy, B. deGlee, J. Liu, M. Liu, An effective strategy to enhancing tolerance to contaminants poisoning of solid oxide fuel cell cathodes, Nano Energy. 47 (2018) 474–480. https://doi.org/10.1016/j.nanoen.2018.03.043.

[11] S.P. Jiang, J.P. Zhang, X.G. Zheng, A comparative investigation of chromium deposition at air electrodes of solid oxide fuel cells, J. Eur. Ceram. Soc. 22 (2002) 361–373. https://doi.org/https://doi.org/10.1016/S0955-2219(01)00280-1.

[12] Y.-L. Huang, A.M. Hussain, C. Pellegrinelli, C. Xiong, E.D. Wachsman, Chromium Poisoning Effects on Surface Exchange Kinetics of La 0.6 Sr 0.4 Co 0.2 Fe 0.8 O 3−δ, ACS Appl. Mater. Interfaces. 9 (2017) 16660–16668. https://doi.org/10.1021/acsami.7b02762.

[13] C. Nicollet, C. Toparli, G.F. Harrington, T. Defferriere, B. Yildiz, H.L. Tuller, Acidity of surface-infiltrated binary oxides as a sensitive descriptor of oxygen exchange kinetics in mixed conducting oxides, Nat. Catal. 3 (2020) 913–920. https://doi.org/10.1038/s41929-020-00520-x.

[14] H.G. Seo, A. Staerz, D.S. Kim, D. Klotz, C. Nicollet, M. Xu, J.M. LeBeau, H.L. Tuller, Reactivation of chromia poisoned oxygen exchange kinetics in mixed conducting solid oxide fuel cell electrodes by serial infiltration of lithia, Energy Environ. Sci. 15 (2022) 4038–4047. https://doi.org/10.1039/D1EE03975J.

[15] Y. Yu, K.F. Ludwig, J.C. Woicik, S. Gopalan, U.B. Pal, T.C. Kaspar, S.N. Basu, Effect of Sr Content and Strain on Sr Surface Segregation of La1-xSrxCo0.2Fe0.8O3-δ as Cathode Material for Solid Oxide Fuel Cells, ACS Appl. Mater. Interfaces. 8 (2016) 26704–26711. https://doi.org/10.1021/acsami.6b07118.

[16] Y. Chen, S. Yoo, Y. Choi, J.H. Kim, Y. Ding, K. Pei, R. Murphy, Y. Zhang, B. Zhao, W. Zhang, H. Chen, Y. Chen, W. Yuan, C. Yang, M. Liu, A highly active, CO2-tolerant electrode for the oxygen reduction reaction, Energy Environ. Sci. 11 (2018) 2458–2466. https://doi.org/10.1039/c8ee01140k.

[17] S.-L. Zhang, H. Wang, M.Y. Lu, A.-P. Zhang, L. V Mogni, Q. Liu, C.-X. Li, C.-J. Li, S.A. Barnett, Cobalt-substituted SrTi0.3Fe0.7O3−δ: a stable high-performance oxygen electrode material for intermediate-temperature solid oxide electrochemical cells, Energy Environ. Sci. 11 (2018) 1870–1879. https://doi.org/10.1039/C8EE00449H.

[18] B. Koo, H. Kwon, Y. Kim, H.G. Seo, J.W. Han, W. Jung, Enhanced oxygen exchange of perovskite oxide surfaces through strain-driven chemical stabilization, Energy Environ. Sci. 11 (2018) 71–77. https://doi.org/10.1039/c7ee00770a.

[19] A. Staerz, H.G. Seo, D. Klotz, D.S. Kim, J.M. Lebeau, The Influence of Cr-Additives on the Polarization Resistance of Praseodymium-Doped Ceria Cathodes for Solid Oxide Fuel Cells, J. Electrochem. Soc. 169 (2022) 044530. https://doi.org/10.1149/1945-7111/ac67b2.

[20] F. Ciucci, C. Chen, Analysis of electrochemical impedance spectroscopy data using the distribution of relaxation times: A Bayesian and hierarchical Bayesian approach, Electrochim. Acta. 167 (2015) 439–454. https://doi.org/10.1016/j.electacta.2015.03.123.

[21] T.H. Wan, M. Saccoccio, C. Chen, F. Ciucci, Influence of the Discretization Methods on the Distribution of Relaxation Times Deconvolution: Implementing Radial Basis Functions with DRTtools, Electrochim. Acta. 184 (2015) 483–499. https://doi.org/10.1016/j.electacta.2015.09.097.

[22] G. Dimitrakopoulos, B. Koo, B. Yildiz, A.F. Ghoniem, Highly Durable C2 Hydrocarbon Production via the Oxidative Coupling of Methane Using a BaFe0.9Zr0.1O3−δ Mixed Ionic and Electronic Conducting Membrane and La2O3 Catalyst, ACS Catal. 11 (2021) 3638–3661. https://doi.org/10.1021/acscatal.0c04888.

[23] M. Lang, C. Bohn, M. Henke, G. Schiller, C. Willich, F. Hauler, Understanding the Current-Voltage Behavior of High Temperature Solid Oxide Fuel Cell Stacks, J. Electrochem. Soc. 164 (2017) F1460–F1470. https://doi.org/10.1149/2.1541713jes.

[24] N. Menzler, F. Tietz, M. Bram, I. Vinke, L. Haart, Degradation Phenomena in SOFCs with Metallic Interconnects, in: Ceram. Eng. Sci. Proc., 2009: pp. 93–104. https://doi.org/10.1002/9780470456309.ch9.

[25] P. Caliandro, A. Nakajo, S. Diethelm, J. Van herle, Model-assisted identification of solid oxide cell elementary processes by electrochemical impedance spectroscopy measurements, J. Power Sources. 436 (2019) 226838. https://doi.org/10.1016/j.jpowsour.2019.226838.

[26] J. Hayd, E. Ivers-Tiffée, Detailed Electrochemical Study on Nanoscaled La 0.6 Sr 0.4 CoO 3-δ SOFC Thin-Film Cathodes in Dry, Humid and CO 2 -Containing Atmospheres , J. Electrochem. Soc. 160 (2013) F1197–F1206. https://doi.org/10.1149/2.026311jes.

[27] M. Kornely, A. Neumann, N.H. Menzler, A. Leonide, A. Weber, E. Ivers-Tiffée, Degradation of anode supported cell (ASC) performance by Cr-poisoning, J. Power Sources. 196 (2011) 7203–7208. https://doi.org/10.1016/j.jpowsour.2010.10.033.

[28] H.G. Seo, Y. Choi, W.C. Jung, Exceptionally Enhanced Electrode Activity of (Pr,Ce)O2−Δ-Based Cathodes for Thin-Film Solid Oxide Fuel Cells, Adv. Energy Mater. 8 (2018) 1–7. https://doi.org/10.1002/aenm.201703647.

[29] E.J. Opila, D.L. Myers, N.S. Jacobson, I.M.B. Nielsen, D.F. Johnson, J.K. Olminsky, M.D. Allendorf, Theoretical and Experimental Investigation of the Thermochemistry of CrO2(OH)2(g), J. Phys. Chem. A. 111 (2007) 1971–1980. https://doi.org/10.1021/jp0647380.

[30] H. Asteman, J.-E. Svensson, M. Norell, L.-G. Johansson, Influence of Water Vapor and Flow Rate on the High-Temperature Oxidation of 304L; Effect of Chromium Oxide Hydroxide Evaporation, Oxid. Met. 54 (2000) 11–26. https://doi.org/10.1023/A:1004642310974.

[31] H. Falk-Windisch, J.E. Svensson, J. Froitzheim, The effect of temperature on chromium vaporization and oxide scale growth on interconnect steels for Solid Oxide Fuel Cells, J. Power Sources. 287 (2015) 25–35. https://doi.org/https://doi.org/10.1016/j.jpowsour.2015.04.040.

[32] M. Stanislowski, E. Wessel, K. Hilpert, T. Markus, L. Singheiser, Chromium Vaporization from High-Temperature Alloys: I. Chromia-Forming Steels and the Influence of Outer Oxide Layers, J. Electrochem. Soc. 154 (2007) A295. https://doi.org/10.1149/1.2434690.

[33] R. Spotorno, D. Paravidino, S. Delsante, P. Piccardo, Volatilization of chromium from AISI 441 stainless steel: Time and temperature dependence, Surf. Coatings Technol. 433 (2022) 128125. https://doi.org/https://doi.org/10.1016/j.surfcoat.2022.128125.

[34] L. Zhao, N.H. Perry, T. Daio, K. Sasaki, S.R. Bishop, Improving the Si impurity tolerance of $Pr_{0.1}Ce_{0.9}O_{2-\delta}$ SOFC electrodes with reactive surface additives, Chem. Mater. 27 (2015) 3065–3070. https://doi.org/10.1021/acs.chemmater.5b00501.

[35] C. Anandan, P. Bera, XPS studies on the interaction of CeO_2 with silicon in magnetron sputtered CeO_2 thin films on Si and Si_3N_4 substrates, Appl. Surf. Sci. 283 (2013) 297–303. https://doi.org/https://doi.org/10.1016/j.apsusc.2013.06.104.

[36] K. Michel, T.S. Bjørheim, T. Norby, J. Janek, M.T. Elm, Importance of the Spin-Orbit Interaction for a Consistent Theoretical Description of Small Polarons in Pr-Doped CeO_2, J. Phys. Chem. C. 124 (2020) 15831–15838. https://doi.org/10.1021/acs.jpcc.0c05352.

[37] S.R. Bishop, T.S. Stefanik, H.L. Tuller, Electrical conductivity and defect equilibria of $Pr_{0.1}Ce_{0.9}O_{2-\delta}$, Phys. Chem. Chem. Phys. 13 (2011) 10165–10173. https://doi.org/10.1039/c0cp02920c.

[38] M. Kilo, Cation Transport in Stabilised Zirconias, Defect Diffus. Forum. 242–244 (2005) 185–254. https://doi.org/10.4028/www.scientific.net/DDF.242-244.185.

[39] N. Sakai, H. Kishimoto, K. Yamaji, T. Horita, M.E. Brito, H. Yokokawa, Interface Stability of Perovskite Cathodes and Rare-Earth Doped Ceria Interlayer in SOFCs, J. Electrochem. Soc. 154 (2007) B1331. https://doi.org/10.1149/1.2789801.

[40] L. Zhou, J.H. Mason, W. Li, X. Liu, Comprehensive review of chromium deposition and poisoning of solid oxide fuel cells (SOFCs) cathode materials, Renew. Sustain. Energy Rev. 134 (2020) 110320. https://doi.org/https://doi.org/10.1016/j.rser.2020.110320.

[41] H.G. Seo, D.H. Kim, J. Seo, S.J. Jeong, J. Kim, H.L. Tuller, J.W. Son, W.C. Jung, High-Performance and Durable Fuel Cells using Co/Sr-Free Fluorite-Based Mixed Conducting $(Pr,Ce)O_{2-\delta}$ Cathode, Adv. Energy Mater. (2022). https://doi.org/10.1002/aenm.202202101.

[42] R. Han, J. Gao, S. Wei, Y. Su, Y. Qin, Development of highly effective $CaO@Al_2O_3$ with hierarchical architecture CO_2 sorbents via a scalable limited-space chemical vapor deposition technique, J. Mater. Chem. A. 6 (2018) 3462–3470. https://doi.org/10.1039/C7TA09960F.

[43] K. Natesan, M. Uz, D.L. Smith, Development of CaO coatings by thermal and chemical vapor deposition, J. Nucl. Mater. 307–311 (2002) 1323–1328. https://doi.org/https://doi.org/10.1016/S0022-3115(02)01225-4.